Journal of Alloys and Compounds 503 (2010) 507–513

Contents lists available at ScienceDirect

Journal of Alloys and Compounds

journal homepage: www.elsevier.com/locate/jallcom

Improvement in electrical stability of ZnO varistors by infiltration of molten Bi_2O_3

Kaiyang Yuan, Guorong Li, Liaoying Zheng*, Lihong Cheng, Lei Meng, Zheng Yao, Qingrui Yin

State Key Laboratory of High Performance Ceramics and Superfine Microstructures, Shanghai Institute of Ceramics, Chinese Academy of Sciences, Shanghai 200050, PR China

ARTICLE INFO

Article history:
Received 6 January 2010
Received in revised form 5 May 2010
Accepted 7 May 2010
Available online 21 May 2010

Keywords:
Ceramics
Oxide materials
Sintering
Diffusion
SEM

ABSTRACT

The infiltration of molten Bi_2O_3 into ZnO varistors was carried out. The sintered varistor disks doped with Bi_2O_3 were painted by Bi_2O_3 paste on the surfaces and then were reheat-treated. The DC degradation test was carried out to demonstrate the electrical stability of varistors. The influence of the Bi_2O_3 infiltration on the electrical nonlinear characteristics and stability of varistors was analyzed by capacitance–voltage (*C–V*) measurements and impedance spectroscopy. The results showed that the Bi_2O_3 infiltration process at temperatures from 800 to 900 °C reduced the donor density in ZnO grains and inhibited the decrease of grain boundary resistance of varistors caused by degradation. The samples infiltrated with Bi_2O_3 at 850 and 900 °C exhibited an excellent electrical stability and maintained relatively high nonlinear characteristics. The enhancement in the electrical stability may be attributed to the diffusion of oxygen into the body of ceramics facilitated by the infiltration of molten Bi_2O_3.

1. Introduction

Zinc oxide varistors are used as reversible, over-voltage protectors with large surge-energy absorption capabilities due to their excellent nonlinear current–voltage (*I–V*) characteristics. A consensus has been reached that the performance of varistors is derived from a double Schottky barrier which forms in the grain boundary regions [1,2]. At present, the majority of commercial varistors are Bi_2O_3-based varistors where Bi_2O_3 is regarded as the primary additive responsible for the varistor behavior. It is well known that Bi_2O_3 has a low melting point (817 °C) and the ZnO–Bi_2O_3 binary system has a eutectic at 750 °C, which give rise to a liquid formation in sintering process. The Bi_2O_3-rich liquid phase wets the ZnO grains boundaries in sintering process, forming intergranular layers, and then recedes to multigrain junction during cooling. As a result, a thin Bi-rich amorphous film (1–2 nm) or intergranular segregation of Bi atoms is left at the ZnO/ZnO grain boundaries, which contributes to the formation of potential barriers [3–7]. The liquid phase facilitates the redistribution of other dopants and the solidified Bi_2O_3-rich phase forms a space network that provides a continuous path for oxygen to diffuse into the material [8].

In practice, however, the electrical degradation of ZnO varistors, leading to a decline of nonlinear characteristics and an increase in leakage current, worsen the performance and limited their useful lives. Therefore, the improvement of the electrical stability is regarded as the most challenge for the further development of varistors. Several mechanisms have been proposed to account for the degradation, including electron trapping, dipole orientation, ion migration and oxygen desorption, among which the ion migration mechanism has been found supportive on the basis of experimental evidences [9–11]. It was believed that the degradation is associated with the migration of the positively charged zinc interstitial ions $Zn_i^{\bullet}$ in the depletion layers [12–16]. According to ion migration mechanism, efforts have previously been made to improve the electrical stability of ZnO varistor by annealing processes at temperatures from 600 to 800 °C [9], and Gupta and Carlson [17] reported the sample heat-treated at 600 °C exhibited the best electrical stability. However, the resultant stability is accompanied by a significant decrease of the nonlinear coefficient of varistors, due to the phase transformation of the intergranular Bi_2O_3 phase (from its initial β or δ to γ phase), indicating that a better method to enhance the electrical stability of ZnO varistors is still necessary.

It is reported that the δ-Bi_2O_3 phase was found in the sample heat-treated at 900 °C [18]. Furthermore, δ-Bi_2O_3 phase was observed to be one of the fastest oxygen-ion conductor, which has led to speculation concerning its role in facilitating varistor stability during heat-treatment in air [8]. However, the heat-treatment above the melting point of Bi_2O_3 will result in its vaporization that yields inferior nonlinear characteristics of varistors [5]. Fortunately, the feasibility of the liquid-infiltration of Bi_2O_3 or Pr_2O_3 into pure ZnO disks or doped samples without Bi_2O_3 or Pr_2O_3 at high temperature has been proved [19–22], which provides a probable method to improve the performance of varistors by the infiltration of molten Bi_2O_3 at high temperature (above 800 °C).

Therefore, the purpose of this paper is to investigate the influence of the Bi_2O_3 infiltration at temperatures from 800 to 950 °C

* Corresponding author. Tel.: +86 21 52412034; fax: +86 21 52413122.
E-mail address: Zhengly@mail.sic.ac.cn (L. Zheng).

0925-8388/$ – see front matter © 2010 Elsevier B.V. All rights reserved.
doi:10.1016/j.jallcom.2010.05.042

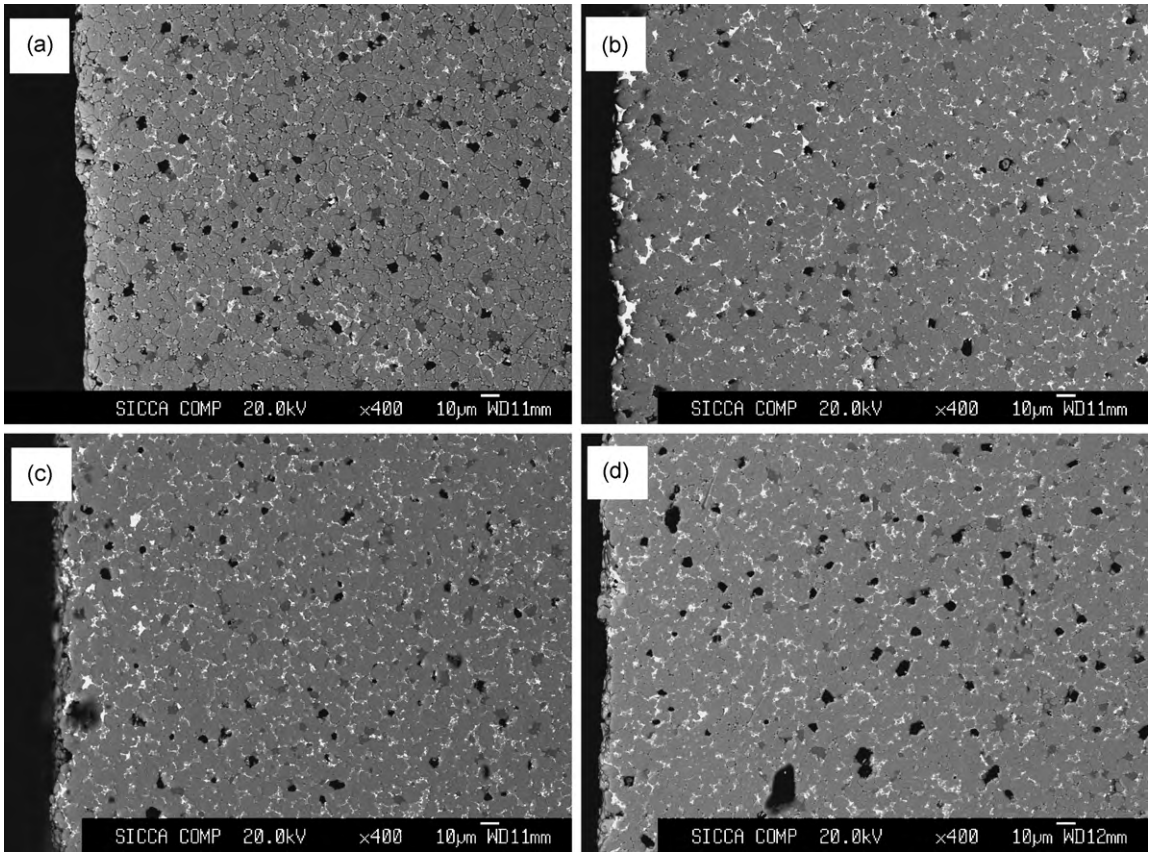

Fig. 1. SEM-BS photographs of the cross-section of ZnO varistor ceramics as-sintered and Bi_2O_3 infiltrated at different temperatures: (a) as-sintered, (b) infiltrated at 850 °C, (c) infiltrated at 900 °C, (d) infiltrated at 950 °C.

on the electrical nonlinear characteristics and stability of ZnO varistors.

2. Experimental

2.1. Sample preparation

The composition of ZnO varistors was 93.29(mol)%ZnO + 0.7%Bi_2O_3 + 1.0%Sb_2O_3 + 0.5%MnO + 1.5%Co_2O_3 + 1.0%NiO + 0.5%Cr_2O_3 + 0.5%SiO_2 + 0.01%Al_2O_3. Raw materials were mixed by ball-milling and then pressed into disks with PVA binder. The green disks were sintered at 1180 °C in air for 1 h and then furnace cooled. The final size of disks was 20 mm in diameter and 1.5 mm in thickness. The disc samples were screened with Bi_2O_3 paste on both parallel planes and were placed on a "V" shape support avoiding the surface of samples touching the support. The alumina crucible was used to cover the samples. The Bi_2O_3 paste was composed of Bi_2O_3 powder and mixed solvent (containing ethyl cellulose, butyl carbitol and ethyl acetate). The disks with Bi_2O_3 paste were fired again in the 800–950 °C temperature range with 50 °C intervals for 1 h in air. After the heat-treatment, the both sides of specimens were polished off 100 μm from the surfaces, and were painted with a silver paste.

2.2. Microstructure

The cross-sections and surfaces of samples selected were polished and then etched in 10 mol/L NaOH solution for 3 min. This method made it possible to preferentially etch the ZnO grains avoiding serious chemical damage to the Bi_2O_3-rich phase. The surfaces of samples selected were polished off 0.2 mm from the top to show the interior microstructure in materials. Scanning electron microscopy in back-scattered mode (SEM-BS) was used to observe the microstructure. In back-scattered electron images, the different composition showed different contrast, and each identified phase was also examined by energy dispersive X-ray spectroscopy (EDS). The area-fraction of Bi_2O_3 phase was calculated using ImageJ software (version 1.43u, Wayne Rasband, National Institute of Health, USA). The XRD was used to identify the different phases (especially for the different Bi_2O_3 phases) in samples as-sintered, infiltrated at 900 °C and infiltrated at 950 °C.

2.3. Measurements of electrical properties

2.3.1. Nonlinear electrical properties

The nonlinear coefficient (α) was determined according to the following equation: $\alpha = (\log J_2 - \log J_1)/(\log E_2 - \log E_1)$, where J_1 = 0.1 mA/cm^2, J_2 = 1.0 mA/cm^2, E_1 and E_2 are the electrical fields corresponding to J_1 and J_2, respectively. The electrical field at the current density of 1 mA/cm^2 was defined as the threshold voltage ($V_{1\,mA}$) and leakage current (I_L) was measured at 0.75$V_{1\,mA}$ (Test Equipment: Keithley 2000 Multimeter, Advantest R8420, Agilent 3312A and Trek 609E-6).

2.3.2. DC stability tests

The DC accelerated aging tests were performed under stress state of 0.85$V_{1\,mA}$/130 °C/10 h (Advantest R8420, DC power supply), where the leakage current was monitored at an interval of 1 min. The degradation rate coefficient (K_T) was determined according to the equation: $I_L = I_{L0} + K_T\sqrt{t}$, where I_{L0} is the initial leakage current at time t = 0 [23]. The lower the degradation rate coefficient, the higher the electrical stability of varistors.

2.3.3. Capacitance–voltage (C–V) measurements

The voltage dependence of capacitance measurements to investigate the Schottky barrier in ZnO varistors were performed at 1 kHz in the bias range 0–40 V using the HP4294 precision impedance analyzer (Agilent, Palo Alto, CA).

2.3.4. Impedance spectra (IS) measurements

The impedance measurements were performed at room temperature using an impedance analyzer (HP4294) in a frequency ranging from 40 Hz to 10 MHz with an amplitude voltage of 0.5 V.

3. Results and discussion

3.1. Changes in microstructure

Fig. 1 shows the back-scattered electron images in cross-section direction of specimens both as-sintered and infiltrated with Bi_2O_3. In the back-scattered mode, the Bi_2O_3-rich phase is identified as

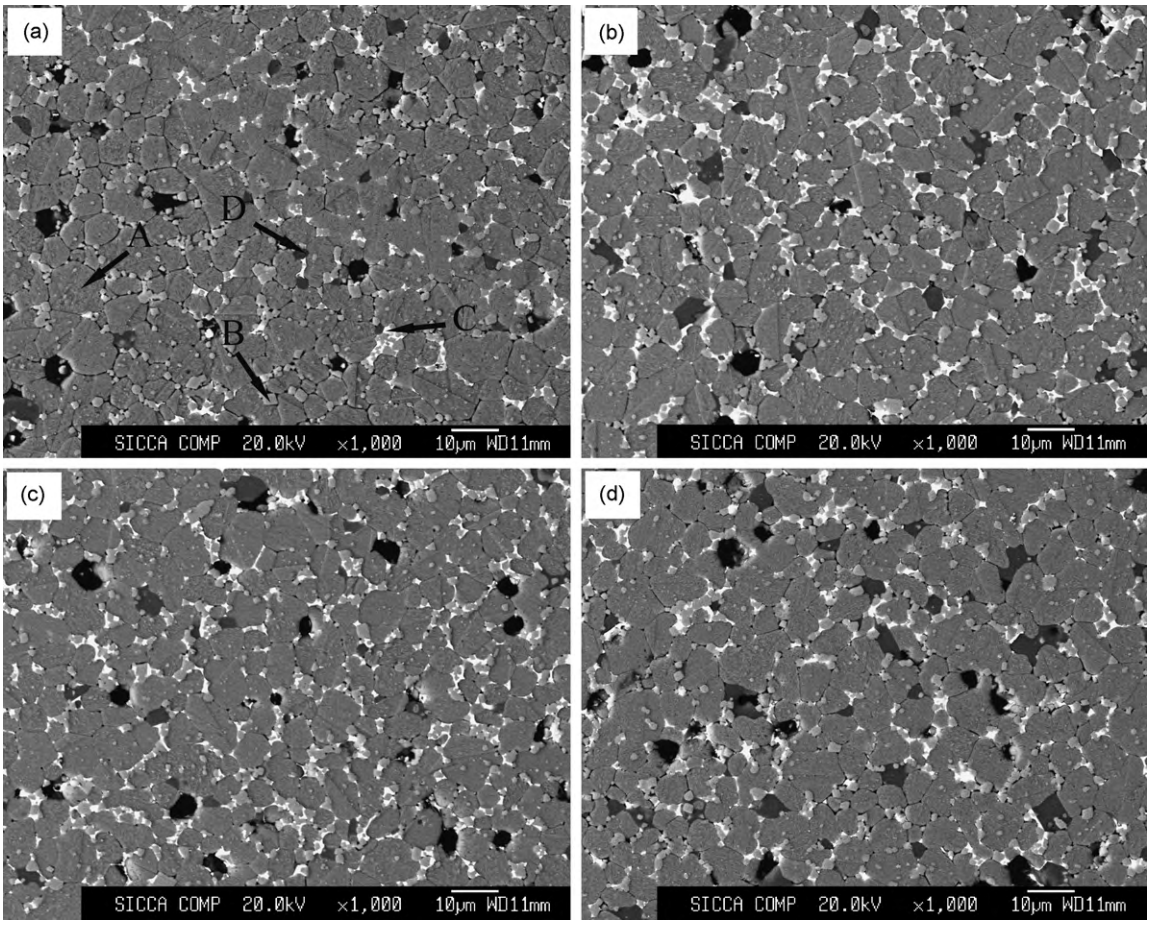

Fig. 2. SEM-BS photographs of the microstructure of ZnO varistor ceramics as-sintered and Bi_2O_3 infiltrated at different temperatures: (a) as-sintered, (b) infiltrated at 850 °C, (c) infiltrated at 900 °C, (d) infiltrated at 950 °C; (A) ZnO grain, (B) $Zn_7Sb_2O_{12}$, (C) Bi-rich phase, (D) Zn_2SiO_4.

bright spots [20]. After Bi_2O_3 infiltration, the remarked increase in the content of Bi_2O_3-rich phase and its improved distribution uniformity clearly indicated that the molten Bi_2O_3 did infiltrate into the interior of the ceramics. Fig. 2 is the back-scattered electron images of the etched surface of specimens. It is observed that the Bi_2O_3-rich phase mainly locates at some two-grain junctions and triple points. The open pores and the triple points of the ZnO grains are believed to provide the main channel for the infiltration of Bi_2O_3 liquid. The composition of the four main phases (ZnO grain, Bi_2O_3-rich phase, $Zn_7Sb_2O_{12}$ spinel and Zn_2SiO_4 spinel) in Fig. 2a was examined by EDS. In addition, the area-fraction of Bi_2O_3 phase in different samples in Fig. 1 was calculated using ImageJ software. The results show that the sample infiltrated at 950 °C gives a lower area-fraction of Bi_2O_3 phase (3.0%) than the ones infiltrated at 850 °C (3.8%) and at 900 °C (3.9%), which may be due to the vaporization of Bi_2O_3 liquid at relatively high temperature. We also checked the back-scattered electron images at high magnification carefully, and no obvious pyrochlore phase, slightly darker in comparison to Bi_2O_3 phase, was observed after Bi_2O_3 infiltration from 800 to 950 °C.

3.2. *I–V* nonlinear characteristics of varistors

Fig. 3 is the *J–E* curves of samples both as-sintered and infiltrated with Bi_2O_3, and the electrical parameters ($V_{1\,mA}$, α, I_L) are listed in Table 1. The results show that the $V_{1\,mA}$ and α are slightly decreased for all the Bi_2O_3 infiltrated samples, while the I_L remarkably increased from 0.7 to 2.1 μA/cm^2, excepting the nonlinear coefficient of the one infiltrated at 950 °C. As a reference, the sintered disk heat-treated without Bi_2O_3 paste at 850 °C was prepared, and the electrical properties are also listed in Table 1. Compared with as-sintered samples, the heat-treated samples without Bi_2O_3 paste have almost the same $V_{1\,mA}$ and I_L values but exhibit much poorer nonlinear behavior (the α value decreases from 41 to 30), whereas all the Bi_2O_3 infiltrated specimens remain relatively high nonlinear coefficients. It is well known that the thin Bi_2O_3-rich amorphous film or segregation of Bi existing in two-grain bound-

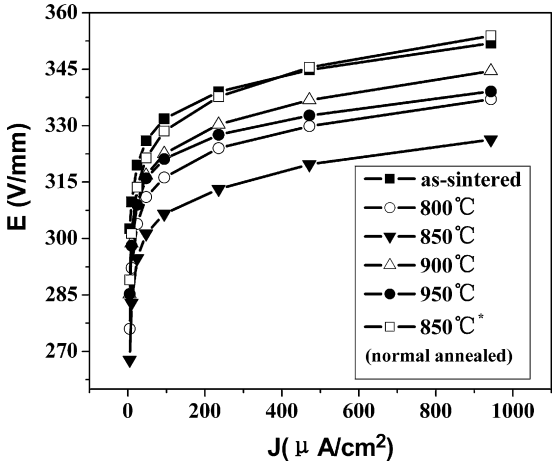

Fig. 3. Current density–electrical field (*J–E*) characteristics of varistors as-sintered, Bi_2O_3 infiltrated at different temperatures and heat-treated without Bi_2O_3 paste at 850 °C (850 °C*).

Table 1
Electrical parameters of ZnO varistor ceramics as-sintered, Bi_2O_3 infiltrated at different temperatures and heat-treated without Bi_2O_3 at 850 °C (850 °C*).

Samples	$V_{1\,mA}$ (V/mm)	I_L (μA/cm²)	α
As-sintered	352	0.7	41
800 °C	338	2.1	39
850 °C	326	1.9	40
900 °C	345	1.6	37
950 °C	340	1.2	44
850 °C*	354	0.7	30

aries, which formed initially by the grain boundary diffusion of Bi_2O_3 fed in part by the network of Bi_2O_3 liquid, plays an important role in the varistor behavior [20]. In heat-treatment process, the infiltration of molten Bi_2O_3 increases the content of liquid phase and facilitates the re-wetting of ZnO grains, probably leading to relatively high nonlinear coefficient after the heat-treatment.

3.3. DC stability of varistors

In an application of varistors, a long-term operation under the bias easily causes the degradation of electrical properties, resulting in a remarkable increase in the leakage current and a decline of the nonlinear electrical characteristics. Further, the resultant joule heat may even cause the loss of the varistor function. Therefore, in addition to the excellent nonlinear characteristics of varistors, the high electrical stability is a prerequisite.

Fig. 4a demonstrates the distinct difference in the electrical stability of as-sintered and Bi_2O_3 infiltrated samples under DC accelerated aging stresses. All the infiltrated samples, except the one infiltrated at 950 °C, reveal a better stability than the as-sintered samples. Particularly, the infiltrated samples at 850 and 900 °C exhibit more flat leakage–current curves and much lower degradation rate coefficients (K_T = 0.032 and 0.034 mA h$^{-1/2}$, respectively) than the as-sintered sample (K_T = 0.251 mA h$^{-1/2}$), suggesting that the electrical stability could be remarkably improved by the infiltration of molten Bi_2O_3. The detailed electrical parameters before and after degradation are summarized in Table 2. The results show that the samples infiltrated at 850 and 900 °C also give small variation rates in threshold voltage, nonlinear coefficient and leakage current ($\%\Delta\alpha$, $\%\Delta V_{1\,mA}$, $\%\Delta I_L$,), which confirms their improved stabilities. To further clarify the influence of the Bi_2O_3 infiltration on the electrical stability, the specimens heat-treated without Bi_2O_3 paste at 850 °C and those infiltrated with Bi_2O_3 at 850 °C are investigated (see Fig. 4b). As expected, the latter exhibits a better stability, showing a slower increase in leakage–current and a more flat leakage–current curve.

3.4. Capacitance–voltage (C–V) characteristics

To explore the probable mechanism for the improvement of the electrical stability by the Bi_2O_3 infiltration process, the capacitance–voltage (C–V) characteristics were applied. Based on the Schottky-barrier model of ZnO varistors, the barrier height (ϕ_b), the donor density (N_d), the interface state density (N_s) and the depletion layer width (t) are obtained by C–V measurements [24,25].

Fig. 5 shows a good linear relationship between $[1/C - 1/(2C_0)]^2$ and applied voltage per grain boundary for all the ZnO varistor samples, and the detailed parameters (ϕ_b, N_d, N_s and t) are summarized in Table 3. It was worth noting that the N_d values in ZnO grains significantly decreased after the Bi_2O_3 infiltration at temperatures from 800 to 900 °C. The variation trend of the N_d is consistent with the result of the electrical stability of varistors, as shown in Fig. 4a and Table 2. Further, the infiltrated sample at 850 °C with the minimum of the N_d value (see Table 3) shows the best stability. As mentioned previously, the zinc interstitial ion $Zn_i^{\bullet}$ is the predominant migrating ion responsible for the electrical degradation, and it is also a donor defect in ZnO grains. Therefore, the improvement in the electrical stability of varistors may be associated with the variation of the donor density. Chen et al. [26] also reported the remarkably decreased in donor density of ZnO grains

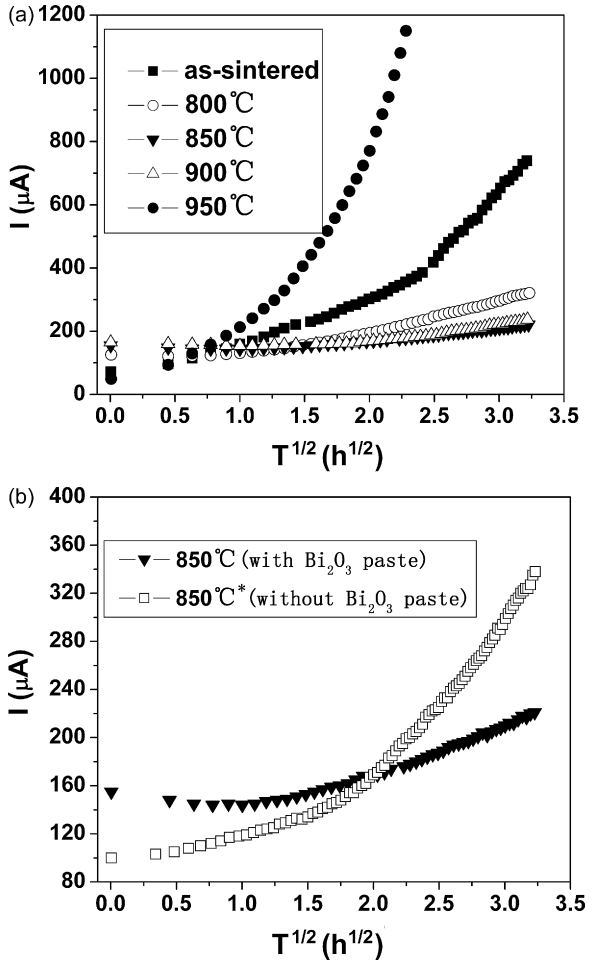

Fig. 4. The leakage current of various ZnO varistors under DC accelerated aging stress: (a) as-sintered and Bi_2O_3 infiltrated at different temperatures, (b) Bi_2O_3 infiltrated at 850 °C and heat-treated without Bi_2O_3 paste at 850 °C (850 °C*).

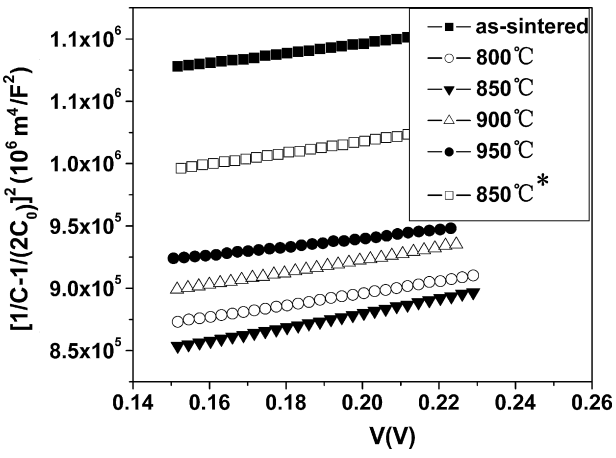

Fig. 5. $[1/C - 1/(2C_0)]^2$ as a function of applied voltage per grain boundary (V) for ZnO varistors as-sintered, Bi_2O_3 infiltrated at different temperatures and heat-treated without Bi_2O_3 paste at 850 °C (850 °C*).

Table 2
The variation of *I–V* characteristic parameters of as-sintered and Bi_2O_3 infiltrated ZnO varistors before and after DC accelerated aging test.

Samples		K_T (mA h$^{-1/2}$)	α	%Δα	$V_{1\,mA}$ (V/mm)	%Δ$V_{1\,mA}$	I_L (μA/cm^2)	%ΔI_L
As-sintered	Before		41		352		0.7	
	After	0.251	21	−48.8	348	−1.1	5.8	728.6
800 °C	Before		39		338		2.1	
	After	0.080	30	−23.1	336	−0.6	6.3	200.0
850 °C	Before		40		326		1.9	
	After	0.032	34	−15.0	326	0	3.1	63.2
900 °C	Before	–	37		345		1.6	
	After	0.034	34	−8.1	344	−0.3	3.2	100.0
950 °C	Before		44		340		1.2	
	After	2.0184	10	−77.3	295	−13.2	24.1	1908.3

of ZnO varistors after heat-treatment at 900 °C in oxygen atmosphere, which was accompanied with improved electrical stability. It is reasonable to speculate that the decrease in the donor density and the enhancement of the electrical stability may be caused by the following process: the Bi_2O_3 infiltration increases the content of Bi_2O_3 phase and completes the continuous space network of solidified Bi_2O_3 phase that acts as the path for oxygen to enter the interior of ceramics. Meanwhile, the δ-Bi_2O_3 phase, the fastest oxygen-ion conductor, exists in the samples after heat-treatment at 850 °C or 900 °C. Both of the completed space network of Bi_2O_3 and δ-Bi_2O_3 phase facilitate the entrance of oxygen into materials. A rapid diffusion of oxygen occurs through the continuous path of solidified Bi_2O_3 phase during heat-treatment process [9], and then the oxygen is absorbed at grain boundaries and captures an electron from a negative charged zinc vacancy due to its high electron affinity, forming a negatively charged adsorbed oxygen (O'_{ad}). Simultaneously, the zinc interstitial ions $Zn_i^{\bullet}$ in ZnO grains diffuse out towards grain boundaries in heat-treatment process, and then reacts with the adsorbed oxygen (O'_{ad}) at the grain boundaries, producing a ZnO lattice. As a result, the interstitial ion $Zn_i^{\bullet}$ is eliminated, which is responsible for the decrease of the donor density and the improvement of the electrical stability. In the reaction, the grain boundary provides a neutral oxygen vacancy and a neutral zinc vacancy. The elimination of $Zn_i^{\bullet}$ can be described as the following reactions:

$$\frac{1}{2}O_2(g) \rightarrow O_{ad}$$

$$O_{ad} + V'_{Zn} \rightarrow O'_{ad} + V^{\times}_{Zn}$$

$$O'_{ad} + V^{\times}_{O} + Zn_i^{\bullet} + V^{\times}_{Zn} \rightarrow ZnO$$

A similar process of elimination of the zinc interstitial ions $Zn_i^{\bullet}$ in heat-treatment process has also been suggested [9,27]. Further, when compared with the sample heat-treated without Bi_2O_3 paste at 850 °C, the Bi_2O_3 infiltrated sample at 850 °C still shows a lower donor density and a better electrical stability (see Fig. 4b and Table 3), confirming the speculation above. Due to the process of the Bi_2O_3 phase transformation is similar for both of the samples above, the lower donor density in the Bi_2O_3 infiltrated sample

Table 3
C–V characteristic parameters of ZnO varistor ceramics.

Samples	ϕ_b (eV)	N_s (10^{16} m^{-2})	N_d (10^{23} m^{-3})	t (10^{-8} m)
As-sintered	2.54	3.15	4.15	7.58
800 °C	1.67	2.33	3.46	6.74
850 °C	1.35	1.93	2.94	6.57
900 °C	1.66	2.28	3.34	6.83
950 °C	2.57	3.44	4.90	7.02
850 °C*	2.00	2.60	3.60	7.23

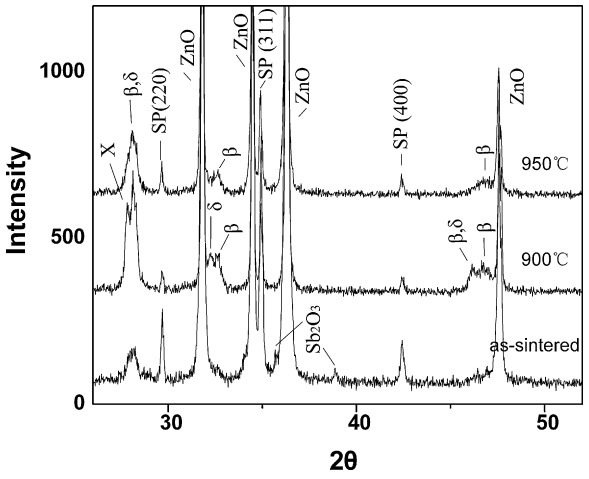

Fig. 6. XRD patterns of ZnO varistors as-sintered and Bi_2O_3 infiltrated at different temperatures. δ: δ-Bi_2O_3, β: β-Bi_2O_3, SP: $Zn_7Sb_2O_{12}$ spinel, *X*: $Bi_{16}CrO_{27}$.

should be only attributed to the completed the Bi_2O_3 network by the Bi_2O_3 infiltration. In addition, based on the presumption above, the aggravated degradation phenomena by further increasing the infiltration temperature up to 950 °C may be owing to the high donor density in ZnO grains (see Table 3). The vaporization of Bi_2O_3 liquid and the phase transformation from δ-Bi_2O_3 to β-Bi_2O_3 [18] after heat-treated at 950 °C may be responsible for the high donor density, resulting to the decline in the capability of the Bi_2O_3 space network to conduct oxygen. Fig. 6 shows the XRD patterns of samples as-sintered, infiltrated at 900 and 950 °C. The obvious peaks of δ-Bi_2O_3 and β-Bi_2O_3 phase appeared in the samples infiltrated at 900 °C, but only obvious β-Bi_2O_3 peak was observed for 950 °C.

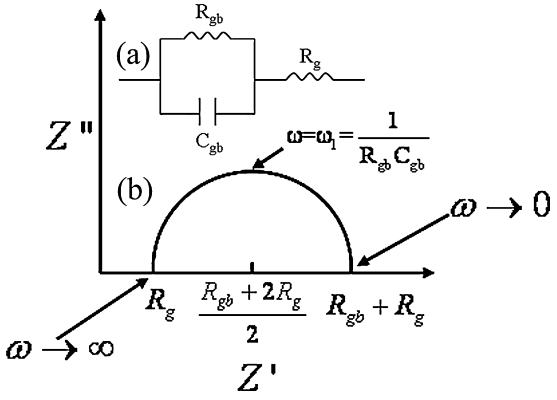

Fig. 7. (a) Typical equivalent circuit and (b) ideal Nyquist plot (Cole–Cole plots) for a ZnO varistor.

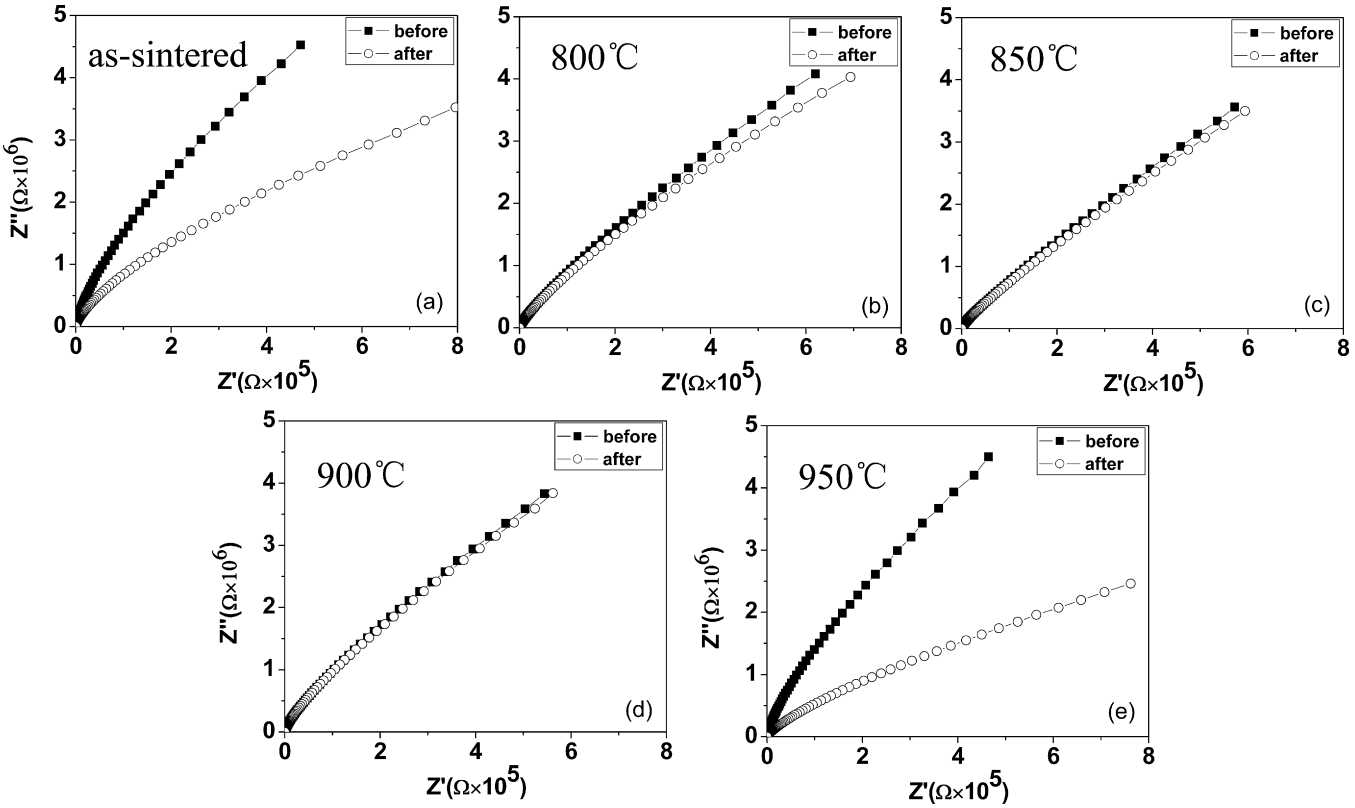

Fig. 8. Impedance Spectra of ZnO varistors at room temperature before and after DC accelerated aging test.

This tendency of phase transition for Bi_2O_3 is similar with Inada's experiment [18].

3.5. Impedance before and after degradation

The IS technique allows for the separation of the main contributions to the electrical conductivity of a polycrystalline solid: bulk (grain) and internal surfaces (grain boundaries) [28]. It is reported that the resistance of the grain boundary would decrease after degradation [29]. Although the reason has not been exactly understood, this result is quite consistent with the fact that the degradation of ZnO is a grain boundary phenomenon.

Fig. 7 shows the typical equivalent circuit and the corresponding ideal Nyquist plot (Cole–Cole plots) proposed by Levinson and Philipp [30] for ZnO varistors (R_g for resistance of the grain, R_{gb} and C_{gb} for resistance and capacitance of the grain boundary, respectively). According to Eq. (1)–(4), the high frequency (left hand side of Fig. 7b) and low frequency (right hand side of Fig. 7b) intercept points of the plots on the real component axis (Z' axis) correspond to R_g and $R_g + R_{gb}$, respectively. Since $R_{gb} \gg R_g$, then $R_g + R_{gb} \approx R_{gb}$.

$$Z = Z' + jZ'' \tag{1}$$

$$Z' = \frac{R_{gb}}{1 + (\omega/\omega_1)^2} + R_g \tag{2}$$

$$Z'' = \frac{-R_{gb}(\omega/\omega_1)}{1 + (\omega/\omega_1)^2} \tag{3}$$

$$(Z'' - 0)^2 + (Z' - \frac{R_{gb} + 2R_g}{2})^2 = \frac{{R_{gb}}^2}{4} \tag{4}$$

The impedance spectra of as-sintered and Bi_2O_3 infiltrated samples before and after degradation are shown in Fig. 8. The complete impedance semicircle is hardly obtained at room temperature for ZnO based varistors, however, the trend of change on the R_{gb} can be still observed. As shown in Fig. 8, the R_{gb} reduces for all the samples after the DC degradation test but shows remarkable difference in the decrease degree. It is observed that the as-sintered sample exhibits an obvious decrease in the R_{gb} value, when compared with those infiltrated with Bi_2O_3 at temperatures from 800 to 900 °C. That confirms the effect of the Bi_2O_3 infiltration process on the enhancement in the electrical stability of varistors. While the serious decrease in R_{gb} of the sample infiltrated at 950 °C is corresponding to its poor electrical stability.

4. Conclusions

The electrical stability of ZnO varistors was remarkably improved by the infiltration of molten Bi_2O_3, and the infiltrated samples also remained relatively high nonlinear coefficients. The results showed that the Bi_2O_3 infiltration process at temperatures from 800 to 900 °C reduced the donor density in ZnO grains and inhibited the decrease of grain boundary resistance of varistors caused by degradation. Compared with others, the Bi_2O_3 infiltrated samples at 850 and 900 °C exhibited the lowest degradation rate. The improvement in the electrical stability of varistors may be attributed to the decrease in the amount of the interstitial ions $Zn_i^{\bullet}$ in ZnO grains due to the diffusion of oxygen into interior of material facilitated by the Bi_2O_3 infiltration process. In addition, the electrical degradation was aggravated when the temperature of the Bi_2O_3 infiltration increased up to 950 °C. That may result from the high donor density in ZnO grains caused by the vaporization of Bi_2O_3 liquid and the phase transformation from δ-Bi_2O_3 to β-Bi_2O_3 after heat-treatment at 950 °C.

Acknowledgements

This work was supported by the NSFC of China (no. 50675218 and no. 10876041), the 973 project of China (no. 2009CB623305).

References

[1] G.D. Mahan, L.M. Levinson, H.R. Philipp, J. Appl. Phys. 50 (1979) 2799–2812.
[2] M. Inada, Jpn. J. Appl. Phys. 19 (1980) 409–419.
[3] E. Olsson, G.L. Dunlop, J. Appl. Phys. 66 (1989) 4317–4324.
[4] K.O. Magnusson, S. Wiklund, J. Appl. Phys. 76 (1994) 7405–7409.
[5] M. Peiteado, M.A. de la Rubia, M.J. Velasco, F.J. Valle, A.C. Caballero, J. Eur. Ceram. Soc. 25 (2005) 1675–1680.
[6] T. Takemura, M. Kobayashi, Y. Takada, K. Sato, J. Am. Ceram. Soc. 69 (1986) 430–436.
[7] W.G. Morris, J. Am. Ceram. Soc. 56 (1973) 360–364.
[8] D.R. Clarke, J. Am. Ceram. Soc. 82 (1999) 485–502.
[9] T.K. Gupta, J. Am. Ceram. Soc. 73 (1990) 1817–1840.
[10] K. Eda, A. Iga, M. Matsuoka, J. Appl. Phys. 51 (1980) 2678–2684.
[11] K. Sato, Y. Takada, T. Takemura, M. Ototake, J. Appl. Phys. 53 (1982) 8819–8826.
[12] T.K. Gupta, A.C. Miller, J. Mater. Res. 3 (1988) 745–754.
[13] M.S. Ramanachalam, A. Rohatgi, J.P. Schaffer, T.K. Gupta, J. Appl. Phys. 69 (1991) 8380–8386.
[14] A. Rohatgi, S.K. Pang, T.K. Gupta, W.D. Straub, J. Appl. Phys. 63 (1988) 5375–5379.
[15] T.K. Gupta, W.D. Straub, M.S. Ramanachalam, J.P. Schaffer, A. Rohatgi, J. Appl. Phys. 66 (1989) 6132–6137.
[16] M.S. Ramanachalam, A. Rohatgi, W.B. Carter, J.P. Schaffer, T.K. Gupta, J. Electron. Mater. 24 (1995) 413–419.
[17] T.K. Gupta, W.G. Carlson, J. Appl. Phys. 53 (1982) 7401–7409.
[18] M. Inada, Jpn. J. Appl. Phys. 18 (1979) 1439–1446.
[19] N.Y. Lee, M.S. Kim, I.J. Chung, M.H. Oh, J. Mater. Sci. 26 (1991) 1126–1130.
[20] M.W. Barsoum, A. Elkind, F.A. Selim, J. Am. Ceram. Soc. 79 (1996) 962–966.
[21] S.Y. Chun, K. Shinozaki, N. Mizutani, J. Mater. Sci. Mater. Electron. 11 (2000) 73–80.
[22] S.Y. Chun, K. Shinozaki, N. Mizutani, J. Am. Ceram. Soc. 82 (1999) 3065–3068.
[23] F. Jiwei, F. Robert, J. Appl. Phys. 77 (1995) 4795–4800.
[24] K. Mukae, K. Tsuda, I. Nagasawa, J. Appl. Phys. 50 (1979) 4475–4476.
[25] C.W. Nahm, J. Eur. Ceram. Soc. 23 (2003) 1345–1353.
[26] C.S. Chen, C.T. Kuo, I.N. Lin, J. Mater. Res. 13 (1998) 1560–1567.
[27] T.K. Gupta, W.G. Carlson, J. Mater. Sci. 20 (1985) 3487–3500.
[28] S.P. Jiang, J.G. Love, S.P.S. Badwal, in: J. Nowotny, C.C. Sorrell (Eds.), Electrical Properties of Oxide Materials, Trans Tech Publications, Clausthal Zellerfe, 1997, pp. 81–132.
[29] S.J. So, C.B. Park, J. Korean Phys. Soc. 40 (2002) 925–929.
[30] L.M. Levinson, H.R. Philipp, Am. Ceram. Soc. Bull. 65 (1986) 639–646.